ACS Catalysis

Research Article

pubs.acs.org/acscatalysis

Effect of Platelet-Shaped Surfaces and Silver-Cation Exchange on the Photocatalytic Hydrogen Production of $RbLaNb_2O_7$

David Arney and Paul A. Maggard*

Department of Chemistry, North Carolina State University, Raleigh, North Carolina 27695-8204, United States

Supporting Information

ABSTRACT: The layered Dion-Jacobsen $RbLaNb_2O_7$ photocatalyst was prepared in platelet-shaped morphologies using a RbCl flux and with a modulation of the particle morphologies using from 1:1−10:1 ($RbCl:RbLaNb_2O_7$) molar ratios and reaction times of 24 h−1 h at a temperature of 1100 °C. Further, the silver-ion exchanged $AgLaNb_2O_7$ product could be prepared by reaction of the $RbLaNb_2O_7$ particles within a $AgNO_3$ flux at 250 °C for 24 h. These products were characterized by powder X-ray diffraction (e.g., *Imma*, a = 5.4763(8) Å, b = 22.4042(2) Å, c = 5.1576(3) Å, for $RbLaNb_2O_7$; $I4_1/acd$, a = 7.7803(2) Å, c = 42.5692(4) Å, for $AgLaNb_2O_7$). At a 10:1 flux ratio, rounded-platelet morphologies with smooth surfaces were observed by scanning electron microscopy (SEM) with thicknesses of ∼100−300 nm and lateral dimensions of ∼1.0−6.0 μm. These particle dimensions and morphologies were conserved during the silver-exchange reactions. Photocatalytic rates for hydrogen production were measured in aqueous methanol and yielded maximal rates for the $AgLaNb_2O_7$ particles of ∼1,457−2,102 μmol H_2 g^{-1} h^{-1} under ultraviolet irradiation and ∼2−20 μmol H_2 g^{-1} h^{-1} under visible irradiation. Photocatalytic rates were generally higher by an order of magnitude or more for the $AgLaNb_2O_7$ particles, with an apparent quantum yield of ∼0.94% at 350 nm. The photocatalytically active areas of the platelets were probed via the photoreduction of Pt islands onto their surfaces, and which revealed preferential deposition onto the particle edges as well as stepped "growth rings" across the particles' faces. These features indicate the confinement of excited electrons to the lateral dimensions of the particles, and thus necessitating them to reach a particle edge or step for a reaction at the particle−solution interface. Electronic-structure calculations based on density functional theory (DFT) show the lowest-energy conduction band states arise from the Nb d-orbital and O p-orbital contributions that are confined to the two-dimensional (2D)-niobate sheets within the structure, and through which the excited-electrons can migrate. The optimum flux synthesis of photocatalyst particles (found at the intermediate 5:1 flux ratio) is found to be a balance between the amount of flux needed to achieve high particle crystallinity, but that does not also lead to well-faceted and smooth surfaces with large lateral dimensions.

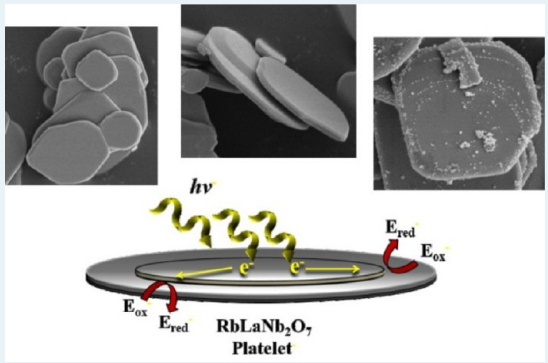

KEYWORDS: *photocatalysis, layered niobate, flux synthesis, silver-cation exchange*

INTRODUCTION

Discovery of new and efficient photocatalytic metal-oxides to convert solar energy into chemical fuels has recently become a rapidly expanding focus of research since the report of the *n*-doped TiO_2 photoelectrode under ultraviolet light.[1−4] Among the many explored photocatalysts, layered metal-oxides have shown much promise in exhibiting some of the highest photocatalytic rates and quantum efficiencies for hydrogen production from water, including $La_2Ti_2O_7$, $Sr_2Ta_2O_7$, $La_4CaTi_5O_{16}$, $HCa_2Nb_3O_{10}$, and $Rb_4Nb_6O_{17}$.[5−13] Additionally, more recent efforts have been aimed toward utilizing the largest fraction of the solar spectrum in the development of efficient visible-light-active photocatalysts for the overall splitting of water.[14−16] It has been shown that Ag-containing early transition-metal oxides can absorb light extending into visible wavelengths as a result of their higher-energy valence bands, but that also remain sufficiently below the (O_2/H_2O) oxidation potential.[15,17−19] A targeted preparation of a layered metal-oxide photocatalyst containing Ag could potentially provide both the high quantum efficiencies and the visible-light absorption necessary for solar-driven hydrogen production from water. To the best of our knowledge this strategy has never previously been investigated.

The $RbLaNb_2O_7$ is a layered Dion−Jacobsen compound that is a photocatalyst under ultraviolet irradiation for water reduction to hydrogen, and also is potentially capable of undergoing ion-exchange reaction with $AgNO_3$ to form $AgLaNb_2O_7$.[20−25] The synthesis of $RbLaNb_2O_7$ has reportedly been performed by only high-temperature solid-state methods, but that typically does not provide a suitable synthetic route to achieving a homogeneous distribution of particle shapes and sizes.[21,22] By contrast, syntheses which utilize molten-salt fluxes

Received: December 8, 2011
Revised: May 29, 2012
Published: July 9, 2012

   dx.doi.org/10.1021/cs200643h | ACS Catal. 2012, 2, 1711−1717

as the reactive media enable a greater control over particle sizes and morphologies through adjusting the flux amount, flux type, reaction temperature, and reaction times. For example, the synthesis of $La_2Ti_2O_7$ particles using a Na_2SO_4/K_2SO_4 eutectic flux yields smaller particle sizes within reaction times of down to ~1 h, and that leads to photocatalytic rates of hydrogen formation nearly two times greater than when prepared by solid-state techniques.[5] Recent investigations into particle surface features and microstructures using flux-synthesis techniques, among a few others, have helped to probe the origins of photocatalytic activity on the surfaces of metal-oxide photocatalysts.[5,14,17,26−32] Thus, it seemed of considerable utility to investigate a two-step synthesis that begins with the flux synthesis of a layered metal oxide, followed by a silver-ion exchange reaction for potential sensitization to visible-light energies.

Presented herein is an investigation of the flux synthesis of $RbLaNb_2O_7$ and its silver ion-exchanged $AgLaNb_2O_7$ product. The flux synthetic conditions were adjusted for optimum reaction times and flux-to-reactant ratios that yielded high purity products and which could be varied to achieve distinguishable particle morphologies and sizes. All products were characterized by powder X-ray diffraction (PXRD), UV−vis diffuse reflectance spectroscopy (DRS), Brunauer−Emmett−Teller (BET) surface area analysis, field emission scanning electron microscopy (FESEM), energy dispersive spectroscopy (EDS), and for their photocatalytic activities for hydrogen production under ultraviolet and visible-light irradiation. Further, the photodeposition of Pt islands onto their surfaces, together with density functional theory (DFT)-based electronic structure calculations, has been used to understand the origins of their changes in photocatalytic rates as well as sensitivity to visible-light.

EXPERIMENTAL DETAILS

Synthesis and Characterization. The flux synthesis of $RbLaNb_2O_7$ was performed by combining a stoichiometric mixture of reagent-grade Rb_2CO_3 (Alfa Aesar, 99%), La_2O_3 (Alfa Aesar, 99.9%, preheated and dried at 900 °C), and Nb_2O_5 (Alfa Aesar, 99.9985%) in a mortar and pestle and grinding well for 30 min prior to the addition of a RbCl (Alfa Aesar, 99.8%, M.P. = 718 °C) flux in flux-to-reactant molar ratios of 1:1, 5:1, and 10:1. After grinding, the reactant mixtures were placed inside alumina crucibles and heated to 1100 °C inside box furnaces with heating times of 1 h, 6 h, and 24 h. Attempts at using a lower reaction temperature resulted in the formation of a $RbNbO_3$ side product. The products were then allowed to radiatively cool to room temperature inside the box furnaces. The resulting powders were then washed with hot deionized (DI) water to remove the flux, and dried overnight at 80 °C. The ion-exchange reaction to give $AgLaNb_2O_7$ was then carried out by mixing the ground $RbLaNb_2O_7$ powders with $AgNO_3$ in a 1:4 molar ratio ($RbLaNb_2O_7$:$AgNO_3$) and heating to 250 °C within alumina crucibles inside a box furnace for 24 h. Fine homogeneous grayish-colored powders of $AgLaNb_2O_7$ were obtained in high purity, as judged by PXRD patterns (Supporting Information). $AgLaNb_2O_7$ was also prepared starting from a $RbLaNb_2O_7$ product made by solid-state techniques, which involved grinding, pelletizing, and heating a stoichiometric mixture of Rb_2CO_3 (20% excess for volatilization), La_2O_3 (preheated), and Nb_2O_5 at 1100 °C for two days, according to the reported literature procedures.[21]

High-resolution PXRD data of all products were collected on an INEL diffractometer using CuKα_1 (λ = 1.54056 Å) radiation from a sealed-tube X-ray generator (35 kV, 30 mA) and a curved position-sensitive detector (CPS120). Unit-cell parameters of the flux-prepared samples were calculated using the LATCON software program.[33] Field-emission scanning electron microscopy analyses were performed on a JEOL SEM 6400, and concomitantly the energy dispersive X-ray (EDX) spectra were taken as a check of the elemental compositions. UV−vis diffuse reflectance spectra (DRS) were collected for all samples on a Shimadzu UV-3600 spectrophotometer equipped with an integrating sphere. BET surface area analyses were performed using a Quantachrome ChemBET Pulsar TPR/TPD. Band-structure calculations of $AgLaNb_2O_7$ and $RbLaNb_2O_7$ were carried out with the use of the plane-wave package CASTEP.[34]

Photocatalysis Measurements. The photocatalytic rates of hydrogen formation for the $MLaNb_2O_7$ (M = Rb, Ag) particles were measured using an outer-irradiation type fused-silica reaction cell with a volume of 90 mL and irradiated under both ultraviolet light (λ > 230 nm) and/or visible light (λ > 400 nm). First, each sample was loaded with a 1 wt % Pt cocatalyst using the standard photochemical deposition methods.[35] Previous studies have shown that platinum islands on metal-oxide surfaces can act as a kinetic aid for the reduction of water to hydrogen.[36] Typically, 200 mg of a $MLaNb_2O_7$ (M = Rb, Ag) sample was mixed with 30 mL of an aqueous solution of dihydrogen hexachloroplatinate(IV) ($H_2PtCl_6{\cdot}6H_2O$; Alfa Aesar, 99.95%), and which was then irradiated for 2 h using a 400W Xe arc-lamp with constant stirring using a magnetic stir bar. A few mL of MeOH was added to each vessel prior to the reaction to aid in the Pt deposition. UV−vis measurements of the remaining solution confirmed a complete deposition of the platinum cocatalyst. After platinization, the particles were separated via centrifugation, washed with deionized water to remove any remaining Cl^- ions, and then dried overnight in an oven at 80 °C. Next, ~50 mg of the platinized $MLaNb_2O_7$ was added to the fused-silica reaction vessel and filled with a 20% aqueous methanol solution. The methanol serves as a hole scavenger, thereby leading to its photo-oxidation to CO_2, and which allows the measurement of the H_2 formation rate alone without the more difficult formation of O_2 as the potentially rate-limiting reaction.[2] The net balanced reaction is $CH_3OH + H_2O \rightarrow 3\ H_2 + CO_2$.

The $MLaNb_2O_7$ particles were first stirred in the dark for ~20−30 min to remove any trapped gases on the particles' surfaces. Next, the reaction cell was irradiated under constant stirring for 6 h using an external 1000 W Xe arc-lamp equipped with an IR water filter and cooled using an external fan. The outlet of the photoreaction vessel was connected to a small horizontal quartz tube that trapped the evolved gases, and contained a moveable liquid bubble that allowed a volumetric determination of the H_2/CO_2 gas mixture at constant pressure. The $MLaNb_2O_7$ samples exhibited the formation of copious amounts of gas bubbles that rose to the top of the reaction cell, and that was observed to be consistent with the movement of the liquid bubble. The progress of the photocatalytic reaction was marked every hour and used to calculate the amount of gases generated in μmol H_2 g^{-1} h^{-1}. The trapped gases were manually injected into a gas chromatograph (SRI MG #2; helium ionization and thermal conductivity detectors) to confirm the generated gases as H_2 and CO_2.

dx.doi.org/10.1021/cs200643h | ACS Catal. 2012, 2, 1711−1717

The Apparent Quantum Yield (AQY) was measured using a reaction cell containing ~35 mg of the 1 wt % platinized $AgLaNb_2O_7$ catalyst and 75 mL of an aqueous 20% MeOH solution that was irradiated using a 400W Xe Arc Lamp equipped with an IR filter and a 350 nm bandpass filter (Newport Oriel), and calculated using the following equation:[35,37]

$$\mathrm{AQY}(\%) = \{[\text{number of reacted electrons}] / [\text{number of incident photons}]\} \times 100$$

The number of reacted electrons was calculated as twice the molar amount of evolved H_2. The number of incident photons was measured on the same reaction vessel using standard ferrioxalate actinometric techniques, described elsewhere.[38]

RESULTS AND DISCUSSION

Syntheses and PXRD. The Dion-Jacobsen $MLaNb_2O_7$ is a layered perovskite containing a double layer of infinite vertex-shared NbO_6 octahedra, and crystallizes in either the orthorhombic space group (*Imma*) for M = Rb or the tetragonal space group ($I4_1/acd$) for M = Ag. The crystal structures for each have been described elsewhere.[20−25] However, $AgLaNb_2O_7$ is a metastable phase that cannot be prepared directly in a single-step solid-state reaction from the constituent oxides. It must be prepared from a silver-exchange reaction with $RbLaNb_2O_7$, and that itself can be prepared by both solid-state and flux-synthetic techniques. The RbCl flux was chosen because the Rb cation is common to $RbLaNb_2O_7$, and this prevents metal-cation competition in the products, it has a relatively low melting point (718 °C), and also is easily removed by washing with hot water after the reaction. In each case, high-purity white-colored powders were formed in as little as 1 h using 10:1, 5:1, and 1:1 molar ratios of RbCl-to-$RbLaNb_2O_7$. Further, all flux-synthesized products could be silver-exchanged to give $AgLaNb_2O_7$ in high purity and yield. In each case, all peaks in the PXRD data could be indexed to the respective crystal structures, and the lattice-constant parameters were refined to consistent values as reported in the literature, given in the Supporting Information, Table S1 and Figure S1. No evidence for any remaining Ag metal, $AgNO_3$ or RbCl flux was present in any of the patterns. Elemental EDX analyses were also performed on both compounds and used to confirm the elemental compositions, Supporting Information, Figures S3 and S4. The spectra revealed Rb, Ag, La, and Nb in their approximate stoichiometric molar ratios

Particle Morphologies and Sizes. The flux-prepared $RbLaNb_2O_7$ and ion-exchanged $AgLaNb_2O_7$ particles were investigated by FESEM techniques. As shown in Figure 1 (a and b), the solid-state preparation of $RbLaNb_2O_7$ and its silver-exchanged $AgLaNb_2O_7$ product formed as aggregates of irregular-shaped platelets with few distinguishable particles. By comparison, the use of small amounts of flux, that is, at the 1:1 (flux:product) molar ratio, resulted in only slightly more distinguishable and somewhat poorly faceted particles similar in size to the solid-state preparation, with dimensions of ~1.0−3.5 μm in Figure 1 (c and d). Further, the low amounts of flux did not result in any increases to the overall surface area, but rather a small decrease in the surface area. At this low flux amount, the reaction is likely flux-assisted, wherein the flux simply aids diffusion at the grain boundaries of the reactants. This is consistent with the observation that a longer reaction time of 6 h (compared to 1 h at a 10:1 ratio) is required to obtain a high-purity synthesis of $RbLaNb_2O_7$ at the 1:1 flux ratio. Ag-exchange reactions of these $RbLaNb_2O_7$ products yielded a significant increase in their surface areas of up to ~2.0−3.8 $m^2 g^{-1}$, but with the same poorly faceted and irregular particle shapes.

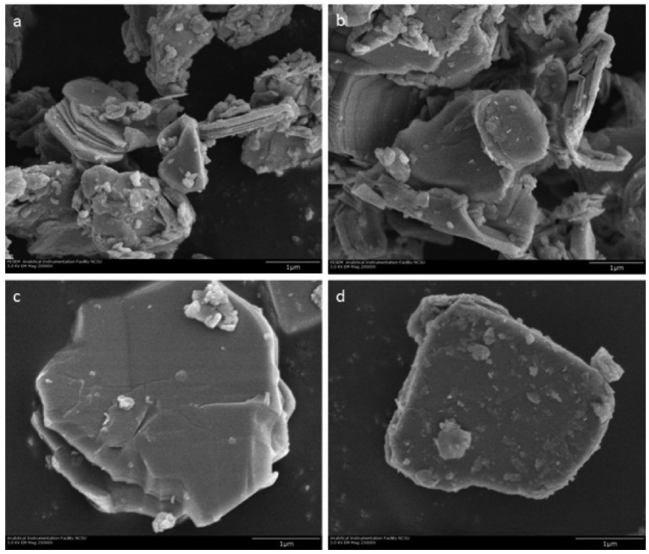

Figure 1. FESEM Images of solid-state prepared $RbLaNb_2O_7$ (a) and after its silver-ion exchange **reaction to** give $AgLaNb_2O_7$ (b); the flux-preparation of $RbLaNb_2O_7$ using a 1:1 RbCl flux (c) and after its silver-ion exchange **reaction to** give $AgLaNb_2O_7$ (d).

When the flux amount is increased to the 10:1 (flux:product) ratio, smooth well-faceted and clearly defined platelet particles are observed with thicknesses of ~100−300 nm and lateral dimensions ranging from ~1.0−6.0 μm, as shown in Figure 2(a and b). This higher flux amount enables the reaction to proceed entirely within the flux, rather than simply at the grain boundaries, and with a shorter reaction time of down to 1 h. A large number of clearly defined nanostepped edges of ~20−100 nm in height was observed near the outer edges of many of the platelet particles, and which occurred perpendicular to the

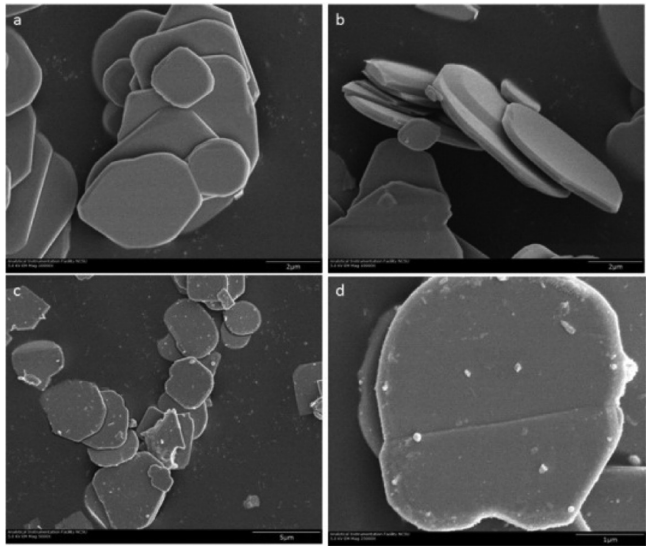

Figure 2. FESEM Images of the flux preparation of $RbLaNb_2O_7$ using a 10:1 RbCl flux (a and b) and after its silver-exchange reaction to give $AgLaNb_2O_7$ (c and d).

dx.doi.org/10.1021/cs200643h | *ACS Catal.* 2012, 2, 1711−1717

platelet faces. These features are consistent with a layer-by-layer particle growth by a Frank-van der Merwe mechanism, wherein a new layer is nucleated at the surface by a nanoadsorbate only after completion of the layer below. No other types of microstructure surface defects could be observed. These $RbLaNb_2O_7$ platelets were silver-exchanged to yield $AgLaNb_2O_7$ platelets that surprisingly were observed to maintain both their platelet dimensions and their overall shapes, shown in Figure 2 (c and d), despite the replacement of all Rb with Ag cations within each particle. The niobate layers within each platelet therefore appear to maintain their registry and stacking during the low-temperature flux-exchange reaction. An overall surface area of ~3.7−3.9 m^2 g^{-1} is found for both the $RbLaNb_2O_7$ and the resultant $AgLaNb_2O_7$ products, and so does not change as a result of the Ag-exchange reaction. Thus, the flux-prepared particles of layered metal oxides may be ion-exchanged, and their particle sizes and features, as well as surface areas, are maintained.

Photocatalytic Hydrogen Production. For the photocatalytic water-splitting reactions, incident photons with energies greater or equal to the bandgap size must be used to excite electrons and create electron/hole pairs, and which then serve as reducing and oxidizing equivalents at the surfaces. The bandgap absorption edges of the $MLaNb_2O_7$ bulk powders were determined by UV−vis diffuse reflectance techniques to be at ~376 nm and ~416 nm for M = Rb and M = Ag, respectively, shown in Figure 3. Optical bandgap sizes (E_g) can

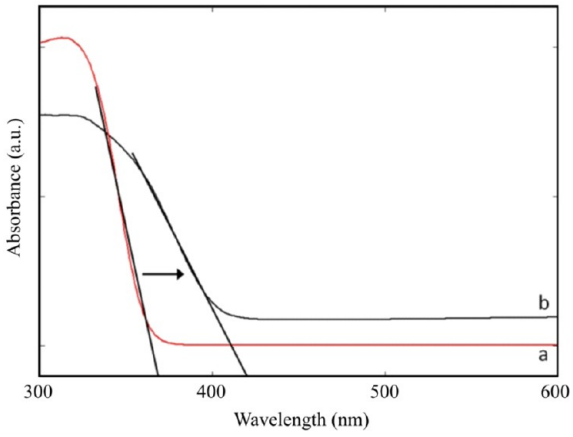

Figure 3. UV−vis diffuse reflectance spectra of flux-prepared $RbLaNb_2O_7$ (a) and after its silver ion-exchange to give $AgLaNb_2O_7$ (b). Reflectance has been converted to absorbance by the Kubelka−Munk method. The arrow indicates the red-shifted absorption edge.

be estimated from the onset of absorption using E_g (eV) = $1240/\lambda_g$ (nm). The $RbLaNb_2O_7$ product has an E_g ~ 3.30 eV, in good agreement with previous reports,[20,25] while $AgLaNb_2O_7$ has a red-shifted E_g ~ 2.98 eV. During the photocatalysis experiment, methanol is typically employed as a sacrificial hole scavenger, while simultaneously measuring the rate of hydrogen production via the reduction of water by excited electrons that reach the surfaces. Photocatalytic rates for hydrogen production in an aqueous methanol solution are listed in Table 1 for each set of $MLaNb_2O_7$ (M = Rb, Ag) particles, either irradiated by visible-light (>400 nm) and/or ultraviolet light, together with the measured surface areas of their bulk powders. A control experiment confirmed no hydrogen is produced from an aqueous methanol solution in the absence of the $MLaNb_2O_7$ photocatalysts under the same conditions. Photocatalytic activity for hydrogen formation was observed in all cases except for $RbLaNb_2O_7$ under visible-light irradiation, and which has a bandgap size that prevents the absorption of lower-energy visible light. Under ultraviolet irradiation, the $RbLaNb_2O_7$ particles exhibited photocatalytic rates at a modest ~70−110 μmol H_2 g^{-1} h^{-1} with either the lowest or highest flux amounts of 1:1 or 10:1 (flux/$RbLaNb_2O_7$). The highest photocatalytic rate for $RbLaNb_2O_7$ was ~373 μmol H_2 g^{-1} h^{-1} for the intermediate 5:1 flux ratio and 24 h reaction (sample D), which had an intermediate surface area of ~1.9 m^2 g^{-1} among the samples.

As described above, the expected behavior of higher photocatalytic rates for higher surfaces was not found. Rather, these data show that particular surface features assist in rendering a metal-oxide particle as more or less active for photocatalytic hydrogen production. The known reaction mechanism for water reduction begins with its adsorption onto the particle surfaces, and which is known to proceed most easily onto stepped edges and defect sites.[39] The most well-faceted and smooth platelets using the highest flux amount (10:1 ratio) yielded lower photocatalysis rates for hydrogen production, as these lack the preferred stepped surfaces for water adsorption. Conversely, the highest photocatalysis rates were found not for the most irregular particles obtained using low flux amounts (1:1 ratio), but which should have the highest amounts of stepped edges. The solid-state route is known to result in particles with lower crystallinity and thus less favorable pathways for electron migration to reach the exposed surfaces. Further, the density of surface defects may be too extensive, and resulting in a more amorphous and disordered surface layer that would inhibit high photocatalytic rates. Rather, an intermediate flux amount is required to enhance the crystallinity of the metal-oxide particles without resulting in completely flat and clean surfaces that lack the stepped edges to be the most photocatalytically active, as further described below. These data show that controlling the density of stepped edges, as well as the crystallinity of the metal oxide particle, are both keys to obtain the most active surfaces and the highest photocatalytic rates for hydrogen production.

The photocatalytic hydrogen production rates of the silver-exchanged $AgLaNb_2O_7$ products under ultraviolet irradiation were higher by an order of magnitude or more than the $RbLaNb_2O_7$ parent particles, as listed in Table 1 and illustrated in Figure 4. The highest photocatalytic rate under ultraviolet irradiation was ~2,102 μmol H_2 g^{-1} h^{-1} for $AgLaNb_2O_7$ (sample A), with an intermediate surface area of ~2.0 m^2 g^{-1} among the different samples. The apparent quantum yield was determined by ferrioxalate actinometry to be ~0.94% at 350 nm. This photocatalytic rate is >30 times higher than its non-exchanged $RbLaNb_2O_7$ counterpart (sample A). The lowest photocatalytic rate for the flux-prepared $AgLaNb_2O_7$ (D) samples was ~1,457 μmol H_2 g^{-1} h^{-1}, and which had a surface area of 3.8 m^2 g^{-1}. This again confirms that particle surface areas here are not the primary determinant of the photocatalytic rates, but rather the amount of active surface areas. We have previously shown that nanostepped surface features can aid in enhancing photocatalytic hydrogen production rates,[5,14,17,26] and which have been investigated in more detail below. Under only visible-light irradiation, all $AgLaNb_2O_7$ samples were found to be photocatalytically active for hydrogen production, though the rates were considerably lower. This is attributed to their absorption edge at ~415 nm that slightly overlaps with the visible-light wavelengths used in the

dx.doi.org/10.1021/cs200643h | ACS Catal. 2012, 2, 1711−1717

Table 1. Photocatalytic Rates of Hydrogen Formation from $RbLaNb_2O_7$ and Silver-Exchanged $AgLaNb_2O_7$ under Visible Light (λ > 400 nm) or Also Including Ultraviolet-Light Irradiation[a]

sample	RbCl:$RbLaNb_2O_7$ flux ratio	reaction time (h)	surface area (m^2/g)	UV-light (μmol H_2/g h)	visible light (μmol H_2/g h)
$RbLaNb_2O_7$ (S.S.)	solid-state[b]	50	1.2	274	
$AgLaNb_2O_7$ (S.S.)	Ag-exchanged		3.8	842	20
$RbLaNb_2O_7$ (A)	1:1	6	0.64	69	
$AgLaNb_2O_7$ (A)	Ag-exchanged		2.0	2102	20
$RbLaNb_2O_7$ (B)	1:1	24	0.71	79	
$AgLaNb_2O_7$ (B)	Ag-exchanged		2.3	1583	10
$RbLaNb_2O_7$ (C)	5:1	6	3.9	111	
$AgLaNb_2O_7$ (C)	Ag-exchanged		3.8	1528	2
$RbLaNb_2O_7$ (D)	5:1	24	1.9	373	
$AgLaNb_2O_7$ (D)	Ag-exchanged		2.7	1806	9
$RbLaNb_2O_7$ (E)	10:1	1	3.9	112	
$AgLaNb_2O_7$ (E)	Ag-exchanged		3.7	1457	15

[a]Photocatalysis Conditions: Outer irradiation 1000 W high-pressure Xe arc-lamp, 50 mg of $MLaNb_2O_7$ (M = Rb, Ag), 20% aqueous MeOH (N_2 purged), and photodeposited 1 wt % Pt surface cocatalyst. [b]Prepared by the solid-state method by heating reactants in absence of any RbCl flux (see Experimental Details).

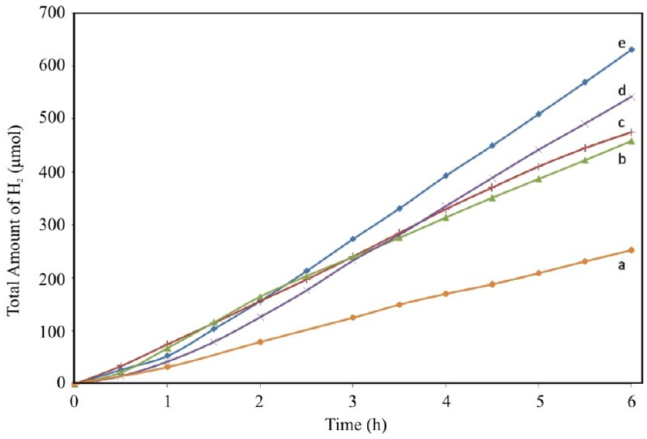

Figure 4. Photocatalytic hydrogen formation versus time for silver-exchanged $AgLaNb_2O_7$ starting from $RbLaNb_2O_7$ when prepared by solid-state methods (a), and by flux methods from a 5:1 RbCl flux reacted for 6 h (b), a 1:1 RbCl flux reacted for 24 h (c), a 5:1 RbCl flux reacted for 24 h (d), and a 1:1 RbCl flux reacted for 6 h (e).

experiment (>400 nm). However, visible-light photocatalytic rates of up to ~20 μmol H_2 g^{-1} h^{-1} were nonetheless observed for $AgLaNb_2O_7$ (sample A), and which also had the highest photocatalytic rate under ultraviolet irradiation. Photocatalytic rates under visible-light irradiation were minimal for the other samples. These results suggest that further sensitization to longer wavelengths would be a promising approach to new photocatalysts.

Photodeposition of Pt Islands and Electronic Structure Calculations. The irradiation of the metal-oxide photocatalyst to drive the photodeposition of a Pt(IV) salt to Pt-metal islands can be used as an aid in determining the amount and location of surfaces with higher reactivity during the photocatalysis experiment.[40,41] Surface features with larger amounts of Pt-islands help indicate the most active surface areas of the particles. The clean and smooth platelet particles of $MLaNb_2O_7$ (M = Rb, Ag) prepared from the 10:1 flux ratio (samples E) were found to be ideal for distinguishing stepped surface features. Several FESEM images were taken after the photochemical deposition of a 5 wt % Pt onto their surfaces, shown in Figure 5 with the Pt islands as white spots. An EDX spot-analysis was used to confirm the chemical composition of the Pt islands, given in the Supporting Information, Figure S2. In addition to the preferential photodeposition of the Pt islands on the outer edges of the particles, they also occur as surprising "growth rings" located over the relatively smooth surfaces of the particles, Figure 5 (c and d). These "growth rings" provide intriguing evidence of nm-scale steps of layers of crystal growth spreading out over the particle surfaces, as would result from the layer-by-layer particle growth by a Frank–van der Merwe mechanism described earlier. Further, the strong preferential photodeposition of Pt islands along these stepped edges is indicative of anisotropy of the excited-electron migration within the planes of these layers, and not perpendicular to them. In contrast, the photodeposition of Pt onto the surfaces of $AgLaNb_2O_7$ particles occurs statistically over all surfaces, shown in Figure 6. It should be noted again that the latter particles exhibit photocatalytic rates that are significantly higher than the smooth $RbLaNb_2O_7$ platelets, and which shows the surface roughness of metal oxides (but with high crystallinity) is key to high photocatalyst rates for hydrogen formation.

Electronic structure calculations were performed on the geometry-optimized structures based on DFT within the CASTEP program package.[34] Shown in Figure 7 (b and c) are plots of the electron densities in the uppermost parts of the valence band, as well as the lowest parts of the conduction band for $AgLaNb_2O_7$. Analogous electron-density plots calculated for $RbLaNb_2O_7$ are provided in the Supporting Information, Figure S6. In both $MLaNb_2O_7$ (M = Ag, Rb), the Nb d-orbital contributions are found at the lowest conduction band energies (i.e., unfilled), that are also mixed with a smaller amount of O p-orbital contributions in a pπ-dπ fashion. However, an analysis of the highest valence-band energies for each shows that while O p-orbital contributions predominate for $RbLaNb_2O_7$ (Supporting Information, Figure S5, b), for $AgLaNb_2O_7$ the Ag d-orbitals mixed with O p-orbital contributions constitute the highest filled states in the valence band, Figure 7c. The calculations show the red-shifted bandgap size of $AgLaNb_2O_7$ arises from the introduction of the higher energy Ag 4d orbitals, and thus the lowest bandgap excitation is a metal-to-metal charge transfer between bands predominantly composed of Ag $4d^{10}$ and Nb $4d^0$ orbitals. Further, the calculations show that the electronic density in the lowest conduction-band states for both $MLaNb_2O_7$ (M = Rb, Ag) are confined to the two-dimensional (2D)-connected niobate layers of the structures.

dx.doi.org/10.1021/cs200643h | ACS Catal. 2012, 2, 1711–1717

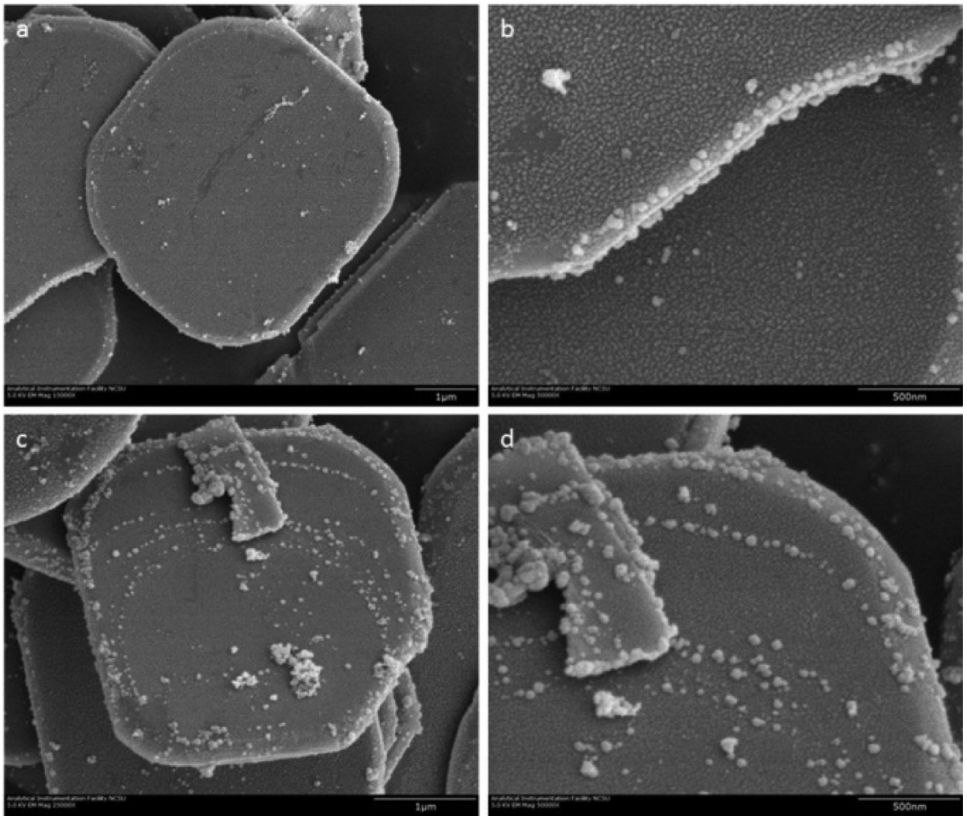

Figure 5. FESEM Images of a 5% wt. platinum photodeposition onto the surfaces of the flux-prepared $RbLaNb_2O_7$ using a 10:1 RbCl flux. Light spots are ∼30−50 nm Pt islands.

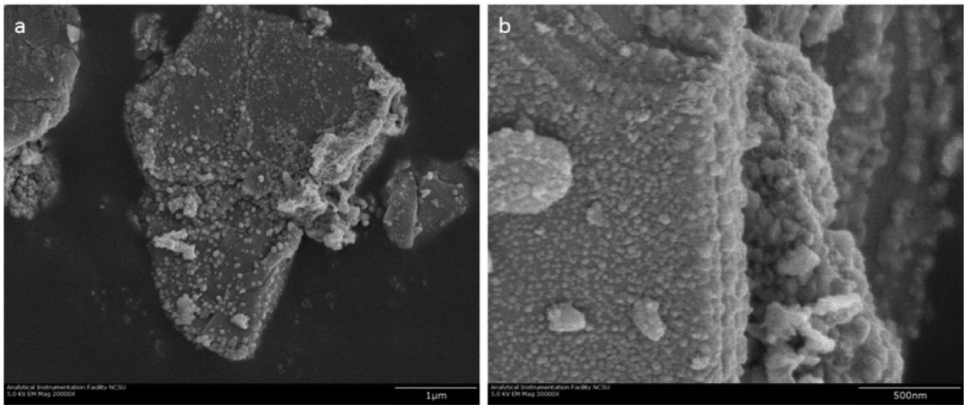

Figure 6. FESEM images of a 5% wt. platinum photodeposition onto the surfaces of $AgLaNb_2O_7$ prepared starting from $RbLaNb_2O_7$ using a 10:1 RbCl flux and followed by a silver-exchange reaction. Light spots are ∼30−50 nm Pt islands.

Thus, these crystal orbitals serve to confine the migration of excited electrons across the lateral dimensions of the particle, until they would arrive at the terminating edges of the platelets. This is consistent with the "growth ring" patterns of photodeposited Pt islands on the surfaces of the well-defined $RbLaNb_2O_7$ platelets, and as well, gives the reason why the highest photocatalytic activities for hydrogen formation should be found for the particles with higher amounts of surface roughness (but also high crystallinity), as described earlier for the flux syntheses.

CONCLUSIONS

The layered photocatalyst $RbLaNb_2O_7$ can be prepared from RbCl-flux reactions with from irregularly shaped to well-defined platelet morphologies with increasing amounts of flux. Low-temperature silver ion-exchange reactions were found to be able to produce $AgLaNb_2O_7$ with good conservation of the particle sizes and morphologies. At high flux amounts, the $MLaNb_2O_7$ platelets exhibited thicknesses of ∼100−300 nm with finer stepped edges down to ∼ <30 nm, and with lateral dimensions from ∼1.0−6.0 μm. These exhibited photocatalytic rates for hydrogen production from aqueous methanol solutions of ∼1,457−2,102 μmol H_2 g^{-1} h^{-1} under ultraviolet irradiation and ∼2−20 μmol H_2 g^{-1} h^{-1} under visible-light irradiation, with a highest apparent quantum yield of 0.94% at 350 nm for $AgLaNb_2O_7$. The highest photocatalytic rates were found for particles that were intermediate between the irregularly shaped morphologies and the well-defined platelets, and that

dx.doi.org/10.1021/cs200643h | *ACS Catal.* 2012, 2, 1711−1717

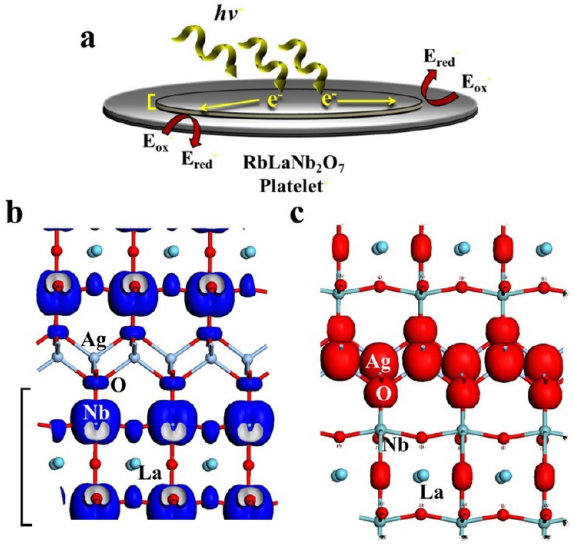

Figure 7. (a) Platelet schematic illustrating the preferential in-plane migration of excited electrons to the stepped edges; Electron-density plots from the calculated electronic structures of $AgLaNb_2O_7$ for the lowest-energy states (blue electron density; unfilled) in the conduction band (b) and the highest-energy states (red electron density; filled) in the valence band (c). The "[" bracket in (b) labels the in-plane migration of electrons in the calculations.

represented a balance between high crystallinity and the occurrence of higher amounts of rough or stepped surfaces. Photodeposited Pt-islands on the well-defined smooth surfaces of the $RbLaNb_2O_7$ platelets were found to exhibit "growth rings", and which illustrated the confinement of excited electrons to the lateral dimensions of these particles, and which thus necessitates them reaching a particle edge or step for reaction in the aqueous solution. Electronic-structure calculations on $RbLaNb_2O_7$ show the lowest-energy conduction band states arise from the Nb d-orbital and O p-orbital contributions that are confined to the 2D-niobate sheets, and along which the electrons must migrate across the lateral dimensions of the particles. Thus, the flux-synthesis of well-defined metal-oxide particles can be used to provide a means to probe the mechanistic origins of photocatalytic hydrogen production, as well as to sensitize them to visible-light energies via subsequent flux-exchange reactions that can conserve their overall particle sizes and morphologies.

■ ASSOCIATED CONTENT

Ⓢ Supporting Information

Refined unit-cell parameters from PXRD patterns for all $MLaNb_2O_7$ (M = Rb, Ag) products, EDX spot analysis of surface Pt islands, representative EDX spectra with calculated elemental compositions, and calculated electron density plots for $RLaNb_2O_7$. This material is available free of charge via the Internet at http://pubs.acs.org.

■ AUTHOR INFORMATION

Corresponding Author

*E-mail: Paul_Maggard@ncsu.edu.

Notes

The authors declare no competing financial interest.

■ REFERENCES

(1) Fujishima, A.; Honda, K. *Nature* **1972**, *238*, 37.
(2) Graetzel, M. E. *Energy Resources through Photochemistry and Catalysis*; Academic Press: New York, 1983.
(3) Domen, K.; Kondo, J.; Hara, M.; Takata, T. *Bull. Chem. Soc. Jpn.* **2000**, *73*, 1307.
(4) Osterloh, F. E. *Chem. Mater.* **2008**, *20*, 35.
(5) Arney, D.; Porter, B.; Greve, B.; Maggard, P. A. *J. Photochem. Photobiol., A* **2008**, *199*, 230.
(6) Hwang, D. W. *J. Catal.* **2000**, *193*, 40.
(7) Hwang, D. W.; Kim, G. H.; Jang, J. S.; Bae, S. W.; Ji, S. M.; Lee, J. S. *Catal. Today* **2004**, *93*, 845.
(8) Hwang, D. W.; Kim, H. G.; Lee, J. S.; Kim, J.; Li, W.; Oh, S. H. *J. Phys. Chem. B* **2005**, *109*, 2093.
(9) Hwang, D. W.; Lee, J. S.; Li, W.; Oh, S. H. *J. Phys. Chem. B* **2003**, *107*, 4963.
(10) Kudo, A. *J. Phys. Chem. B* **2000**, *104*, 571.
(11) Kato, H.; Kudo, A. *J. Photochem. Photobiol., A* **2001**, *145*, 129.
(12) Hyun, G.; Kim, D. W. H.; et al. *Chem. Commun.* **1999**, *12*, 1077.
(13) Sayama, K.; Arakawa, H.; Domen, K. *Catal. Today* **1996**, *28*, 175.
(14) Arney, D.; Watkins, T.; Maggard, P. A. *J. Am. Ceram. Soc.* **2011**, *94*, 1483.
(15) Kudo, A.; Kato, H.; Tsuji, I. *Chem. Lett.* **2004**, *33*, 1534.
(16) Maeda, K.; Teramura, K.; Lu, D.; Saito, N.; Inoue, Y.; Domen, K. *J. Phys. Chem. C* **2007**, *111*, 7554.
(17) Arney, D.; Hardy, C.; Greve, B.; Maggard, P. A. *J. Photochem. Photobiol. A* **2010**, *214*, 54.
(18) Kato, H.; Kobayashi, H.; Kudo, A. *J. Phys. Chem. B* **2002**, *106*, 12441.
(19) Konta, R.; Kato, H.; Kobayashi, H.; Kudo, A. *Phys. Chem. Chem. Phys.* **2003**, *5*, 3061.
(20) Maeda, K.; Mallouk, T. E. *J. Mater. Chem.* **2009**, *19*, 4813.
(21) Gopalakrishnan, J.; Bhat, V.; Raveau, B. *Mater. Res. Bull.* **1987**, *22*, 413.
(22) Hermann, A. T.; Wiley, J. B. *Mater. Res. Bull.* **2009**, *44*, 1046.
(23) Sato, M.; Watanabe, J.; Uematsu, K. *J. Solid State Chem.* **1993**, *107*, 460.
(24) Porob, D. G.; Maggard, P. A. *Chem. Mater.* **2007**, *19*, 970.
(25) Domen, K.; Ebina, Y.; Sekine, T.; Tanaka, A.; Kondo, J.; Hirose, C. *Catal. Today* **1993**, *16*, 479.
(26) Joshi, U. A.; Palasyuk, A.; Arney, D.; Maggard, P. A. *J. Phys. Chem. Lett.* **2010**, *1*, 2719.
(27) Chiu, C.; Li, C.; Desu, S. B. *J. Am. Ceram. Soc.* **1991**, *74*, 38.
(28) Arendt, R. H. *J. Solid State Chem.* **1973**, *8*, 339.
(29) El-Toni, M. A.; Yin, S.; Sato, T. *Mater. Lett.* **2006**, *60*, 185.
(30) Kan, Y.; Jin, X.; Wang, P.; Li, Y.; Cheng, Y.-B.; Yan, D. *Mater. Res. Bull.* **2003**, *38*, 567.
(31) Porob, D. G.; Maggard, P. A. *Mater. Res. Bull.* **2006**, *41*, 1513.
(32) Porob, D. G.; Maggard, P. A. *J. Solid State Chem.* **2006**, *179*, 1727.
(33) Schwarzenbach, D. *Acta Crystallogr., Sect. A* **1989**, *A45*, 63.
(34) Payne, M. C.; Teter, M. P.; Allan, D. C.; Arias, T. A.; Joannopoulos, J. D. *Rev. Mod. Phys.* **1992**, *64*, 1045.
(35) Kato, H.; Asakura, K.; Kudo, A. *J. Am. Chem. Soc.* **2003**, *125*, 3082.
(36) Nakamatsu, H.; Kawai, T.; Koreeda, A.; Kawai, S. *J. Chem. Soc., Faraday Trans. 1* **1986**, *82*, 527.
(37) Kudo, A.; Miseki, Y. *Chem. Soc. Rev.* **2009**, *38*, 253.
(38) Hatchard, C. G.; Parker, C. A. *Proc. R. Soc. London, Ser. A* **1956**, *235*, 518.
(39) Bard, A. J.; Dekker, M. *Encyclopedia of the Electrochemistry of the Elements*; Appleby, A. J., Chemla, H., Kita, H., Bronoël, Eds.; Marcel Dekker: New York, 1982; Vol. *IXA*, p 383.
(40) Kraeutler, B.; Bard, A. J. *J. Am. Chem. Soc.* **1978**, *100*, 4317.
(41) Ohtani, B.; Iwai, K.; Nishimoto, S.-i.; Sato, S. *J. Phys. Chem. B* **1997**, *101*, 3349.